

# Linear Catadioptric Camera Calibration from Sphere Images

Xianghua Ying, Hongbin Zha  
National Laboratory on Machine Perception  
Peking University, Beijing, 100871 P.R.China  
{xhying, zha}@cis.pku.edu.cn

## Abstract

*A spherical object has been introduced into central catadioptric camera calibration through utilizing the properties of an image conic, which is the projection of the occluding contour of a sphere in the catadioptric image. However, previous calibration method using sphere images employs nonlinear optimization method and requires a good initial estimation to start the minimization. In this paper, we propose a novel linear approach to this problem. The main contribution of this paper is that we discovered that each sphere image is tangent to the modified image of the absolute conic (MIAC) at two double-contact image points, and a linear calibration method using sphere images is derived from this observation. The linear algorithm has been tested in extensive experiments with respect to noise sensitivity.*

## 1. Introduction

Catadioptric camera systems are often employed in many computer vision applications, including robot navigation, virtual reality, image-based rendering, etc. Recently, Baker and Nayar [3] investigated these catadioptric systems with respect to a single viewpoint constraint. The catadioptric systems can be classified into two classes, central and noncentral, depending on whether they keep single viewpoint or not. This paper aims at the calibration of central catadioptric cameras. Many approaches to catadioptric camera calibration have been proposed and they can be classified into three categories: using a calibration pattern with control points [2], self-calibration [10], and using projections of lines [4], [6], [7], [14] or projections of spheres [14].

As discussion in [14], although lines and spheres are all projected into conics in the central catadioptric image plane (A conic from a line is called a *line image*, and a conic from a sphere is called a *sphere image* in this paper.), it is more difficult to extract the projection of a line with high accuracy than that of a sphere. As we know, the accuracy of the estimated intrinsic

parameters highly depends on the accuracy of the extracted conics. Therefore, sphere images are preferred in the case where accurate calibration of central catadioptric cameras is needed. However, the previous calibration method using sphere images [14] employs nonlinear optimization method and requires a good initial estimation to start the minimization. This paper proposes a novel linear approach to this problem, which is drawn inspiration from the study on the conventional camera calibration using sphere images.

The image of the absolute conic (IAC) plays a central role in camera calibration. Teramoto and Xu [12] first discovered the algebraic relation between the sphere image and the IAC under a conventional camera, and then provided an efficient algorithm to solve for the camera parameters. However, in their approach the minimization is accomplished by means of a general-purpose nonlinear minimization and required a good initial estimation to start the minimization. Agrawal and Davis [1] utilized the dual representation instead, i.e., the algebraic relation between the dual form of a sphere image and the dual image of the absolute conic (DIAC), then employed semi-definite programming (SDP) to solve for the intrinsic parameters without requiring initial estimations. Base on the main principles derived in [12] and [1], we further discovered that each sphere image is tangent to the IAC at two double-contact image points, and a linear calibration method using sphere images is derived from this observation as described in [15].

This paper extended the method for conventional camera calibration using sphere images proposed in [15] to deal with catadioptric camera calibration. Similar to a sphere image from a conventional camera which is tangent to the IAC at two points, we discovered that each sphere image from central catadioptric camera is also tangent to an image conic with purely imaginary points, called the modified image of the absolute conic (MIAC, its definition is described in the main text), at two double-contact image points. Then a linear catadioptric camera

calibration method using sphere images is derived from this observation as similar to [15].

## 2. Notations and Basic Principles

### 2.1. Pinhole Camera Model

Let  $\mathbf{M} = [X \ Y \ Z \ 1]^T$  be a world point and  $\mathbf{m} = [u \ v \ 1]^T$  be its image point, both in the homogeneous coordinates, they satisfy,

$$\mu \mathbf{m} = \mathbf{P} \mathbf{M}, \quad (1)$$

where  $\mathbf{P}$  is a  $3 \times 4$  projection matrix describing the perspective projection process.  $\mu$  is an unknown scale factor. The projection matrix can be decomposed as:

$$\mathbf{P} = \mathbf{K} [\mathbf{R} \ | \ \mathbf{t}], \quad (2)$$

where

$$\mathbf{K} = \begin{bmatrix} f_x & s & u_0 \\ 0 & f_y & v_0 \\ 0 & 0 & 1 \end{bmatrix}. \quad (3)$$

Here the upper triangular matrix  $\mathbf{K}$  is the matrix of the intrinsic parameters, and  $(\mathbf{R}, \mathbf{t})$  denote a rigid transformation (i.e.,  $\mathbf{R}$  is a rotation matrix and  $\mathbf{t}$  is a translation vector) which indicate the orientation and position of the camera with respect to the world coordinate system.

### 2.2. A Generalized Image Formation Model for Central Catadioptric Cameras

Geyer and Daniilidis [8] proposed a generalized image formation model for central catadioptric cameras, and proved that the central catadioptric image formation is equivalent to a two-step mapping via a sphere (see Figure 1):

**Step 1:** A point in 3D space is projected to a point on a unit sphere centered at the single effective viewpoint. The unit sphere is called the viewing sphere.

**Step 2:** The point on the viewing sphere is perspectively projected to a point on the image plane  $\Pi$  from another point  $O_C$ . The image plane  $\Pi$  is perpendicular to the line determined by the single viewpoint  $O$  and  $O_C$ .

This step can be considered as taking image of the viewing sphere using a virtual camera whose optical center is located at  $O_C$  and whose optical axis coincides with the line determined by  $O$  and  $O_C$ . We denote the distance  $l = |OO_C|$ . If the intrinsic matrix of the virtual camera is:

$$\mathbf{K}_C = \begin{bmatrix} f_x & s & u_0 \\ 0 & f_y & v_0 \\ 0 & 0 & 1 \end{bmatrix} \quad (4)$$

then from (1) and (2), we have,

$$\mu \mathbf{m}_C = \mathbf{P}_C \mathbf{M}_C, \quad (5)$$

and

$$\mathbf{P}_C = \mathbf{K}_C [\mathbf{I} \ | \ \mathbf{0}], \quad (6)$$

where  $\mathbf{P}_C$  and  $\mathbf{M}_C$  are represented in the camera coordinate system, and  $\mathbf{m}_C$  is represented in the catadioptric image coordinate system.

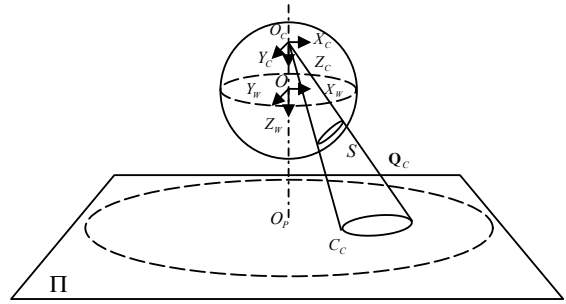


**Figure 1.** A sphere image  $C_C$  under a catadioptric imaging model

### 2.3. The Equation of a Sphere Image

Since  $l=1$  cannot perform catadioptric camera calibration from sphere images [14], we only discuss the cases where  $0 \leq l < 1$  in this paper. Note that  $l=1$  represents a paracatadioptric camera, and  $l=0$  corresponds to a pinhole camera [8].

For a space viewed by a central catadioptric camera, it is projected into a small circle  $S$  on the viewing sphere in the first step (see Figure 1). The equation of the plane containing the small circle  $S$  in the world coordinate system (its origin is located in the center of the viewing sphere  $O$ ) is:

$$n_x X_w + n_y Y_w + n_z Z_w + d_0 = 0, \quad (7)$$

where  $(n_x \ n_y \ n_z)^T$  is the unit normal vector and  $|d_0|$  is the distance from the origin  $O$  to the plane. The projection center  $O_C$  and the small circle  $S$  form a cone (it may be not a right cone) and the equation for the cone in the camera coordinate system is:

$$\mathbf{Q}_C = \begin{bmatrix} (1-l^2)n_x^2 - (d_0 + l \cdot n_z)^2 & (1-l^2)n_x n_y & (l \cdot d_0 + n_z)n_x & 0 \\ (1-l^2)n_x n_y & (1-l^2)n_y^2 - (d_0 + l \cdot n_z)^2 & (l \cdot d_0 + n_z)n_y & 0 \\ (l \cdot d_0 + n_z)n_x & (l \cdot d_0 + n_z)n_y & -d_0^2 + n_z^2 & 0 \\ 0 & 0 & 0 & 0 \end{bmatrix} \quad (8)$$

Then a point  $\mathbf{M}_C = [X_C \ Y_C \ Z_C \ 1]^T$  on the cone  $\mathbf{Q}_C$  in the camera coordinate system satisfies:

$$\mathbf{M}_C^T \mathbf{Q}_C \mathbf{M}_C = 0, \quad (9)$$

or

$$\overline{\mathbf{M}}_C^T \overline{\mathbf{Q}}_C \overline{\mathbf{M}}_C = 0, \quad (10)$$

where  $\overline{\mathbf{M}}_C = [X_C \ Y_C \ Z_C]^T$  are the inhomogeneous coordinates of  $\mathbf{M}_C$ , and

$$\overline{\mathbf{Q}}_C = \begin{bmatrix} (1-l^2)n_x^2 - (d_0 + l \cdot n_z)^2 & (1-l^2)n_x n_y & (l \cdot d_0 + n_z)n_x \\ (1-l^2)n_x n_y & (1-l^2)n_y^2 - (d_0 + l \cdot n_z)^2 & (l \cdot d_0 + n_z)n_y \\ (l \cdot d_0 + n_z)n_x & (l \cdot d_0 + n_z)n_y & -d_0^2 + n_z^2 \end{bmatrix} \quad (11)$$

From (5), the image point of  $\mathbf{M}_C$  satisfies:

$$\mu \mathbf{m}_C = \mathbf{P}_C \mathbf{M}_C = \mathbf{K}_C [\mathbf{I} | \mathbf{0}] \mathbf{M}_C = \mathbf{K}_C \overline{\mathbf{M}}_C. \quad (12)$$

Since  $\mathbf{K}_C$  is invertible, we obtain,

$$\overline{\mathbf{M}}_C = \mu \mathbf{K}_C^{-1} \mathbf{m}_C. \quad (13)$$

Substituting (13) into (10), we have,

$$\mathbf{m}_C^T \mathbf{K}_C^{-T} \overline{\mathbf{Q}}_C \mathbf{K}_C^{-1} \mathbf{m}_C = 0, \quad (14)$$

or

$$\lambda \mathbf{C}_C = \mathbf{K}_C^{-T} \overline{\mathbf{Q}}_C \mathbf{K}_C^{-1}, \quad (15)$$

where  $\lambda$  is an unknown scale factor.  $\mathbf{C}_C$  is the sphere image.

## 2.4. The IAC and the DIAC

The absolute conic  $\Omega_\infty$  is a conic with purely imaginary points on the plane at infinity  $\pi_\infty = [0 \ 0 \ 0 \ 1]^T$ , and its matrix form is:

$$\Omega_\infty = \begin{bmatrix} 1 & 0 & 0 \\ 0 & 1 & 0 \\ 0 & 0 & 1 \end{bmatrix}. \quad (16)$$

The mapping between  $\pi_\infty$  and its perspective image is given by the planar homography  $\mathbf{H} = \mathbf{K}_C \mathbf{R}$ . Since the absolute conic  $\Omega_\infty$  is on  $\pi_\infty$ , one may compute the image of the absolute conic (IAC) under  $\mathbf{H}$  as:

$$\omega_C = \mathbf{H}^{-T} \Omega_\infty \mathbf{H}^{-1} = (\mathbf{K}_C \mathbf{R})^{-T} \mathbf{I} (\mathbf{K}_C \mathbf{R})^{-1} = \mathbf{K}_C^{-T} \mathbf{K}_C^{-1} \quad (17)$$

We may define the dual image of the absolute conic (DIAC) as:

$$\omega_C^* = \mathbf{K}_C \mathbf{K}_C^T. \quad (18)$$

## 2.5. The MIAC and the DMIAC

**Definition 1.** A intrinsic matrix defined as

$$\tilde{\mathbf{K}}_C = \begin{bmatrix} f_x / \sqrt{1-l^2} & s / \sqrt{1-l^2} & u_0 \\ 0 & f_y / \sqrt{1-l^2} & v_0 \\ 0 & 0 & 1 \end{bmatrix}, \quad (19)$$

is called a modified intrinsic matrix.

Obviously,  $\tilde{\mathbf{K}}_C$  and  $\mathbf{K}_C$  satisfy,

$$\tilde{\mathbf{K}}_C = \mathbf{K}_C \begin{bmatrix} 1/\sqrt{1-l^2} & 0 & 0 \\ 0 & 1/\sqrt{1-l^2} & 0 \\ 0 & 0 & 1 \end{bmatrix}. \quad (20)$$

The modified image of the absolute conic (MIAC) satisfies,

$$\tilde{\omega}_C = \mathbf{H}_C^{-T} \Omega_\infty \mathbf{H}_C^{-1} = (\tilde{\mathbf{K}}_C \mathbf{R})^{-T} \Omega_\infty (\tilde{\mathbf{K}}_C \mathbf{R})^{-1} = \tilde{\mathbf{K}}_C^{-T} \tilde{\mathbf{K}}_C^{-1}. \quad (21)$$

We may define the dual of the modified image of the absolute conic (DMIAC) as:

$$\tilde{\omega}_C^* = \tilde{\mathbf{K}}_C \tilde{\mathbf{K}}_C^T. \quad (22)$$

## 3. Algebraic Interpretation

### 3.1. The Algebraic Relation between a Sphere Image and the MIAC

Expanding the right side of (15) using

$$\overline{\mathbf{Q}}_C = -\frac{(d_0 + l \cdot n_z)^2}{(1-l^2)} \begin{bmatrix} 1-l^2 & 0 & 0 \\ 0 & 1-l^2 & 0 \\ 0 & 0 & 1 \end{bmatrix} + \begin{bmatrix} (1-l^2)n_x^2 & (1-l^2)n_x n_y & (l \cdot d_0 + n_z)n_x \\ (1-l^2)n_x n_y & (1-l^2)n_y^2 & (l \cdot d_0 + n_z)n_y \\ (l \cdot d_0 + n_z)n_x & (l \cdot d_0 + n_z)n_y & (l \cdot d_0 + n_z)^2 / (1-l^2) \end{bmatrix} \quad (23)$$

we obtain,

$$\lambda \mathbf{C}_C = \tilde{\omega}_C - \mathbf{v}_C \mathbf{v}_C^T, \quad (24)$$

where  $\tilde{\omega}_C$  is the MIAC, and

$$\mathbf{v}_C = \frac{1-l^2}{d_0 + l \cdot n_z} \tilde{\mathbf{K}}_C^{-T} \begin{bmatrix} n_x \\ n_y \\ (l \cdot d_0 + n_z) / (1-l^2) \end{bmatrix}. \quad (25)$$

### 3.2. The Algebraic Relation between a Sphere Image and the DMIAC

Inverse both side of (15), using

$$\begin{aligned} \bar{\mathbf{Q}}_C^{-1} &= \begin{bmatrix} n_x^2 - 1 + d_0^2 & n_x n_y & (l \cdot d_0 + n_z) n_x \\ n_x n_y & n_y^2 - 1 + d_0^2 & (l \cdot d_0 + n_z) n_y \\ (l \cdot d_0 + n_z) n_x & (l \cdot d_0 + n_z) n_y & (1 - l^2)(-1 + d_0^2) + (l \cdot d_0 + n_z)^2 \end{bmatrix} \\ &= (-1 + d_0^2) \begin{bmatrix} 1 & 0 & 0 \\ 0 & 1 & 0 \\ 0 & 0 & (1 - l^2) \end{bmatrix} + \\ &\quad \begin{bmatrix} n_x^2 & n_x n_y & (l \cdot d_0 + n_z) n_x \\ n_x n_y & n_y^2 & (l \cdot d_0 + n_z) n_y \\ (l \cdot d_0 + n_z) n_x & (l \cdot d_0 + n_z) n_y & (l \cdot d_0 + n_z)^2 \end{bmatrix} \end{aligned} \quad (26)$$

and after some manipulations, we obtain,

$$\lambda' \mathbf{C}_C^* = \tilde{\omega}_C^* - \mathbf{v}'_C \mathbf{v}'_C^T, \quad (27)$$

where  $\lambda'$  is an unknown scale factor, and  $\mathbf{C}_C^*$  is the inversion of the conic  $\mathbf{C}_C$ , i.e., the dual conic.  $\tilde{\omega}_C^*$  is the DMIAC, and

$$\mathbf{v}'_C = \frac{1}{\sqrt{(1 - d_0^2)(1 - l^2)}} \tilde{\mathbf{K}}_C \begin{bmatrix} n_x \\ n_y \\ (l \cdot d_0 + n_z) \end{bmatrix}. \quad (28)$$

From (24) and (27), it is not difficult to find that the two equations have the same mathematical form, no matter whether the dual representation is adopted or not. In the rest of paper, we only discuss the geometric interpretation for  $\tilde{\omega}_C$  and how to determine  $\tilde{\omega}_C$  from this geometric interpretation, because  $\tilde{\omega}_C^*$  can be interpreted and determined in the same way.

### 4. Geometric Interpretation

Equation (24) can be rewritten as:

$$\lambda \mathbf{C}_C - \tilde{\omega}_C = -\mathbf{v}_C \mathbf{v}_C^T. \quad (29)$$

The rank of the matrix  $-\mathbf{v}_C \mathbf{v}_C^T$  is one, therefore, the rank of the matrix  $\lambda \mathbf{C}_C - \tilde{\omega}_C$  is also one. Consider the pencil of two conics  $\mathbf{S}_1$  and  $\mathbf{S}_2$ ,  $\mathbf{S}_1 + \mu \mathbf{S}_2$  represents a conic which passes through all the common points of  $\mathbf{S}_1$  and  $\mathbf{S}_2$  [11]. Since two coincident lines (i.e., a repeated line) can be considered as a degenerate conic with rank 1, from the properties of a pencil of two conics introduced in [11], we know that  $\mathbf{C}_C$  is tangent to  $\tilde{\omega}_C$  at two points,  $\mathbf{m}_I$  and  $\mathbf{m}_J$ , and the line

$\mathbf{l}_C \propto \mathbf{v}_C$  passes through the two tangent points,  $\mathbf{m}_I$  and  $\mathbf{m}_J$  (see Figure 2).

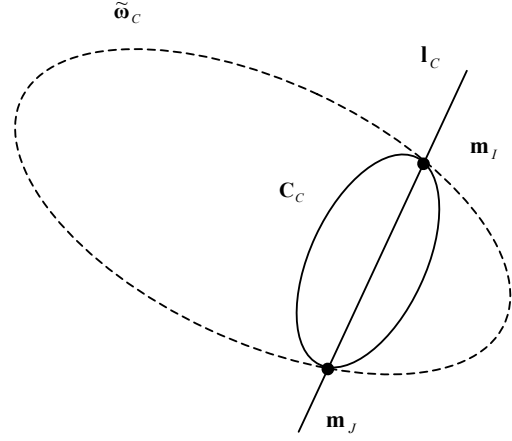


Figure 2. The geometric interpretation of the relation between a sphere image  $\mathbf{C}_C$  and the MIAC  $\tilde{\omega}_C$ .

## 5. Camera Calibration

### 5.1. Determining the MIAC using the Geometric Interpretation

For each sphere image  $\mathbf{C}_C$ , its corresponding line  $\mathbf{l}_C \propto \mathbf{v}_C$  can be determined (How to find  $\mathbf{v}_C$  up to an unknown scale factor has been given in [1], i.e.,  $\|\mathbf{v}_C\|$  is yet unknown). Therefore, the two intersection points of the obtained line  $\mathbf{l}_C$  and the original conic  $\mathbf{C}_C$ , i.e.,  $\mathbf{m}_I$  and  $\mathbf{m}_J$ , can be obtained (see Figure 2). From discussion in Section 4, we know that the two intersection points  $\mathbf{m}_I$  and  $\mathbf{m}_J$  also lie on the MIAC  $\tilde{\omega}_C$ . Therefore, six points on  $\tilde{\omega}_C$  can be obtained from three image conics. Since five points define a conic, the six points are sufficient to estimate  $\tilde{\omega}_C$ . As we know, the MIAC should be positive definite. The linear methods may fail in the case where the computed MIAC is not positive definite. However, this did not occur in our experiments, except in the case where the noises are large. After obtaining  $\tilde{\omega}_C$ , It is not difficult to determine  $\mathbf{v}_C$ , i.e.,  $\|\mathbf{v}_C\|$  from (29).

## 5.2. The Complete Calibration Algorithm using the Geometric Interpretation

The complete calibration algorithm using the geometric interpretation consists of the following steps:

1. Fit conic curves, then obtain  $C_{C_i}$ .
2. Find  $I_{C_i} \propto v_{C_i}$ .
3. Find the intersection points of  $C_{C_i}$  and  $I_{C_i}$ , then determine  $\tilde{\omega}_C$ .
4. If  $\tilde{\omega}_C$  is not positive definite, then stop.
5. Obtain  $\tilde{K}_C$  by using the Cholesky factorization of  $\tilde{\omega}_C$ . Then  $K_C$  may be obtained from  $\tilde{K}_C$  using (21).
6. Obtain  $v_{C_i}$ , then solve for the extrinsic parameters of the camera. (See [12], [13] and [1] for details).

## 6. Experiments

We perform a number of experiments, both simulated and real, to test our algorithms with respect to noise sensitivity, and make comparisons with the following algorithms:

- **GEO** and **DGEO**: Using the geometric interpretation related to the MIAC and the DMIAC, respectively.
- **SDP** and **DSDP**: Employing semi-definite programming with the representation of the MIAC and the DMIAC, respectively [1].

In the real experiments, we use a perspective camera with a hyperbolic mirror, designed by the Center for Machine Perception, Czech Technical University, its field of view (FOV) is 217.2 degree, and the parameter of the hyperbolic mirror is  $l = 0.966$ . Here we assume that the parameter  $l$  is known in advance.

### 6.1. Calibration with Simulated Data

The simulated catadioptric camera has the following parameters:  $f_x = 450$ ,  $f_y = 450$ ,  $s = 0$ ,  $u_0 = 400$ ,  $v_0 = 300$  and  $l = 0.966$ . The resolution of the simulated image is  $800 \times 600$ . We generate an image containing three sphere images uniformly distributed within the image as shown in Figure 3. On each sphere image we choose 100 points. Gaussian noise with zero-mean and  $\sigma$  standard deviation is added to these image points. We vary the noise level  $\sigma$  from 0 to 2 pixels. The conic fitting algorithm presented in [5] is used here. For each noise level, we perform 1,000 independent trials, and the mean values and standard deviations of these recovered parameters are computed over each run. The estimated results of these

experiments are shown in Figure 4. Since the performances of  $f_x$  and  $f_y$ ,  $u_0$  and  $v_0$  are both very similar, the estimated results for  $f_y$  and  $v_0$  are not shown here. From Figure 4, it is not difficult to find that there are only very small differences among the estimated results from these four different methods. We compare the runtimes of these methods using MATLAB implementations of all algorithms on a 1.7 GHz Pentium IV processor. Note that real-time performance is not expected for any of the algorithms under MATLAB, and our only goal is to provide comparison. All results are averaged over 1,000 trials and recorded in Table 1. Since SDP is a convex optimization problem and has polynomial worst-case complexity, the runtimes of **SDP** and **DSDP** are about ten times slower than that using **GEO** and **DGEO**.

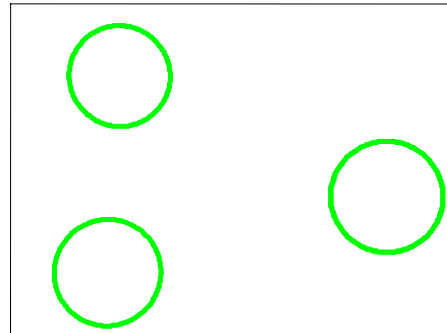


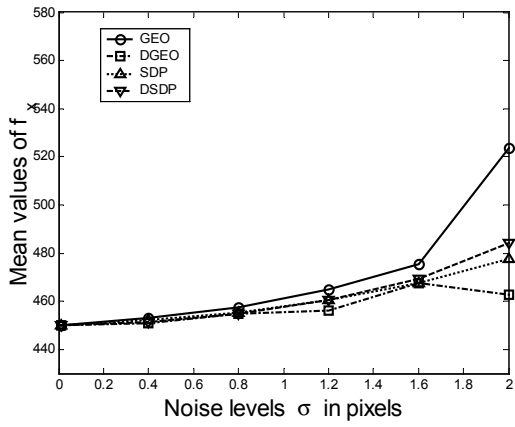
**Figure 3.** The simulated image containing three catadioptric sphere images

**Table 1.** Runtimes (in milliseconds) for the four algorithms

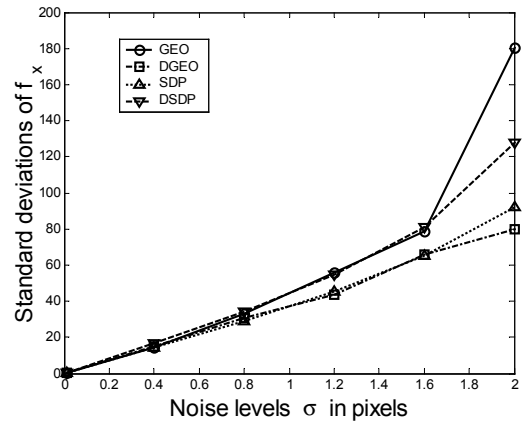
	<b>GEO</b>	<b>DGEO</b>	<b>SDP</b>	<b>DSDP</b>
runtime	93.1	99.2	1598.7	1632.1

**Table 2.** Calibration results with real data

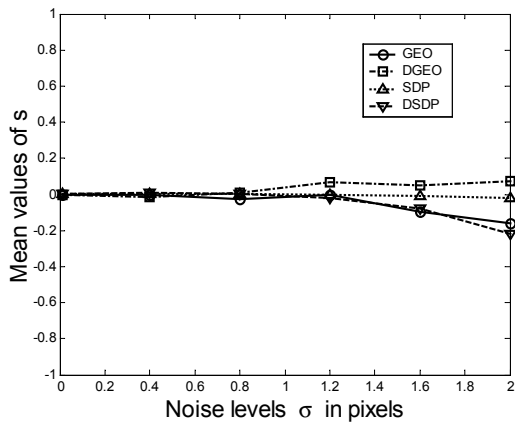
	$f_x$	$f_y$	$s$	$u_0$	$v_0$
<b>GEO</b>	216.3	220.5	5.3	407.0	271.4
<b>DGEO</b>	215.8	220.1	5.5	405.4	274.3
<b>SDP</b>	215.6	219.8	5.3	408.2	269.6
<b>DSDP</b>	217.3	221.6	5.3	410.5	271.4



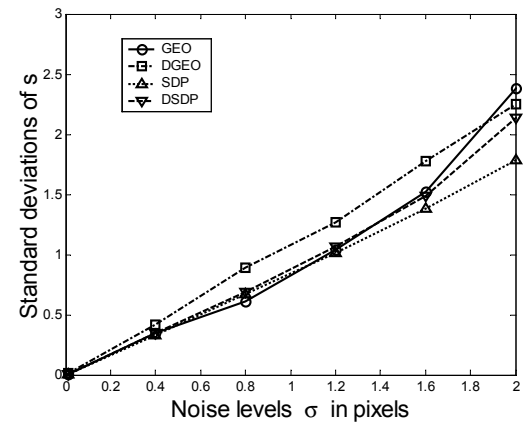
(a)



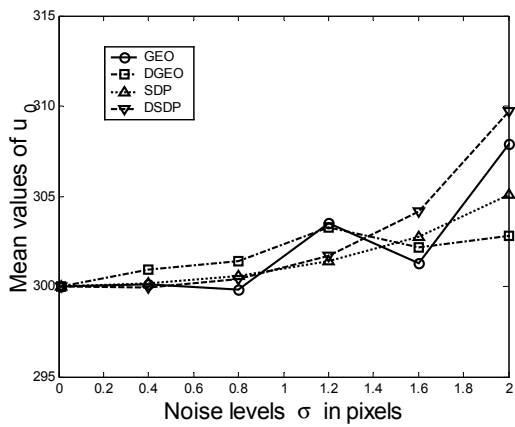
(b)



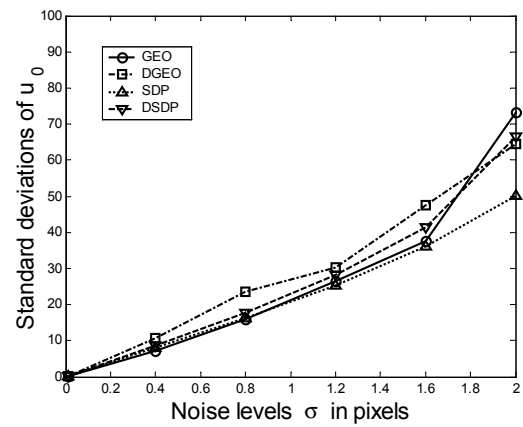
(c)



(d)



(e)



(f)

Figure 4. The estimated results of simulated experiments. See text for details.



**Figure 5.** A sphere image using in the real experiments.

## 6.2. Calibration with Real Data

The test sphere for the real experiments is a billiard ball. The ball was placed in front of a white screen. We took images of the ball using the catadioptric camera. Three sphere images are taken for the calibration purpose. One of the three images is shown in Figure 5. The resolution of these images is  $800 \times 600$ . Edges were extracted using Canny's edge detector and the ellipses were obtained using a least squares ellipse fitting algorithm [5]. In order to obtain unbiased results, these sphere images should be uniformly distributed within the image. The calibration results with real data are listed in Table 2. From Table 2, one may find that the calibration results using these four methods are similar to one another.

## 7. Discussions

In this paper, we discovered that a sphere image and the MIAC are mutually tangent at two double-contact image point. This observation provides new insights into the fundamental properties of a sphere image, especially from the aspect of it providing constraints on the camera parameters. A linear catadioptric camera calibration approach using sphere images is derived from this observation. Only three sphere images are required, and all five intrinsic parameters are recovered linearly without making assumptions, such as, zero-skew or unitary aspect ratio. As we know, the MIAC should be positive definite. The linear methods may fail in the case where the computed MIAC is not positive definite. However, this did not occur in our experiments, except in the case where the noises are large. Extensive experiments on simulated and real data were performed and shown that our calibration method is an order of magnitude faster than previous optimized methods while maintaining comparable accuracy. Finding a novel linear approach from the double-contact theorem is our future work.

## Acknowledgements

This work was supported in part by the NSFC Grant (No. 60333010), and NKBRPC (No. 2004CB318000).

## References

- [1] M. Agrawal, L. S. Davis, "Camera calibration using spheres: A semi-definite programming approach," *Proc. of ICCV*, pp. 782–791, 2003.
- [2] D.G. Aliaga, "Accurate Catadioptric Calibration for Real-time Pose Estimation of Room-size Environments", *In Proc. International Conference on Computer Vision*, Canada, 2001, pp. 127-134.
- [3] S. Baker and S.K. Nayar, "A Theory of Catadioptric Image Formation", *In Proc. International Conference on Computer Vision*, India, 1998, pp. 35-42.
- [4] J.P. Barreto and H. Araújo, "Geometric Properties of Central Catadioptric Line Images", *In Proc. European Conference on Computer Vision*, 2002, pp. 237-251.
- [5] A. Fitzgibbon, M. Pilu, and R. Fisher, "Direct least-square fitting of ellipses", *In Proc. International Conference on Pattern Recognition*, 1996, pp. 253–257.
- [6] C. Geyer and K. Daniilidis, "Catadioptric camera calibration", *In Proc. International Conference on Computer Vision*, 1999, pp. 398–404.
- [7] C. Geyer and K. Daniilidis, "Paracatadioptric Camera Calibration", *IEEE Transactions on Pattern Analysis and Machine Intelligence*, 2002, 24(5): pp. 687-695.
- [8] C. Geyer and K. Daniilidis, "A Unifying Theory for Central Panoramic Systems and Practical Implications," *In Proc. European Conference on Computer Vision*, 2000, pp. 445-462.
- [9] R. Hartley and A. Zisserman, *Multiple View Geometry in Computer Vision*. Cambridge University Press, 2000.
- [10] S.B. Kang, "Catadioptric self-calibration", *In IEEE Conference on Computer Vision and Pattern Recognition*, 2000, pp. 201–207.
- [11] J. Semple and G. Kneebone, *Algebraic Projective Geometry*, Oxford Science Publication, 1952.
- [12] H. Teramoto, G. Xu, "Camera calibration by a single image of balls: From conics to the absolute conic," *Proc. of ACCV*, pp. 499–506, 2002.
- [13] X. Ying, Z. Hu, "Spherical Objects based Motion Estimation for Catadioptric Cameras," *Proc. of ICPR*, Vol. 3, pp. 231-234, 2004.
- [14] X. Ying, Z. Hu, "Catadioptric Camera Calibration Using Geometric Invariants," *IEEE Trans. PAMI*, 26(10), pp. 1260-1271, 2004.
- [15] X. Ying, H. Zha, "Linear Approaches to Camera Calibration from Sphere Images or Active Intrinsic Calibration using Vanishing Points," *To appear in Proc. of ICCV, 2005*.